

Formation of optical flux lattices for ultra cold atoms

G. Juzeliūnas^a and I. B. Spielman^b

^aInstitute of Theoretical Physics and Astronomy, Vilnius University,
A. Goštauto 12, Vilnius LT-01108, Lithuania;

^bJoint Quantum Institute, National Institute of Standards and Technology,
and University of Maryland, Gaithersburg, Maryland, 20899, USA

ABSTRACT

We explore the optical flux lattices produced for ultra-cold atoms in the radiation field when both the atom-light coupling and the detuning exhibit an oscillatory behavior. We analyze not only the magnetic flux but also the geometric vector potential generating the flux, as well as the accompanying geometric scalar potential. We show how to deal with the gauge-dependent singularities of the Aharonov-Bohm (AB) type appearing in the vector potentials for the optical flux lattices. We present a way to calculate the continuous magnetic flux through the elementary cell via the singularities of the vector potential inside the cell. The analysis is illustrated with a square optical flux lattice. We present a way of creating such a lattice using the Raman transitions induced by a set of properly chosen polarization-dependent standing waves propagating at a right angle and containing a time-phase difference.

Keywords: Ultracold atoms, light-induced gauge potentials, optical flux lattices

1. INTRODUCTION

Over the recent years there has been a great deal of interest in artificial gauge fields for ultracold atomic gases.¹ The atomic quantum gases are systems where the condensed matter meets the atomic physics. The atomic gases can exhibit a number condensed matter phenomena,²⁻⁵ such as the Mott transition⁶ or Berezinskii-Kosterlitz-Thouless crossover.⁷ Yet the atoms forming the quantum gases are electrically neutral species and there is no vector potential term governing their center of mass motion. The vector potential type coupling providing a Lorentz force is essential for the magnetic phenomena in solids, such as the quantum Hall effect.⁸ A standard way to produce an artificial magnetic field is to rotate an atomic cloud so that a vector potential term appears in the rotating frame of reference.^{9,10} During the last several years various schemes have been proposed to create an effective magnetic field for ultra-cold atoms without rotation. There are two major groups of these schemes.

The first group relies on an optical lattice which traps atoms at its sites. The magnetic flux is simulated by inducing an asymmetry in the atomic tunneling between the lattice sites, so that an atom picks up a non-zero phase after completing a closed loop along a plaquette.¹¹⁻¹⁷ Such an asymmetry can be induced by means of the laser-assisted tunneling^{11-14,16} or using time-dependent lattices.^{13,15,17}

The second group of proposals is based on the concept of geometric gauge potentials which are encountered in many areas of physics.¹⁸⁻²⁵ In the context of the atomic gases the geometric vector and scalar potentials were first considered in the late 90's for atoms interacting with the laser fields.²⁶⁻²⁸ The approach involves a concept of atomic states “dressed” by the laser beams. It is the position dependence of these dressed internal states which leads to the emergence of the geometric vector and scalar potentials. The method can provide a non-zero effective magnetic field using non-trivial spatial arrangements of laser fields²⁹⁻³⁴ or position-dependent detuning of the atom-light coupling.³⁵⁻³⁷ In these approaches the effective magnetic flux over the atomic cloud linearly increase with the cloud dimensions.^{31,33,35,36} This is an obstacle in reaching the magnetic fluxes which are high enough to observe the fractional Hall effect³⁸ for ultra-cold atoms.

Recently it was shown that the magnetic flux produced by the geometric potentials can be made proportional to the surface area of the atomic cloud and thus be considerably increased,³⁹ see also.⁴⁰ For this it was suggested to use a two-level model of the atom-light coupling in which both the atom-light coupling and the detuning exhibit an oscillatory position-dependence. Using this approach one not only generates a non-staggered magnetic flux but also produces a lattice potential thus providing an optical flux lattice.³⁹ It is instructive that

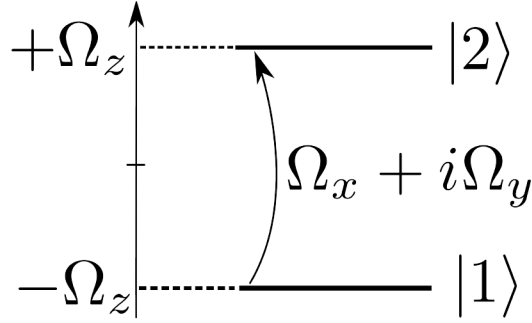


Figure 1. Two-level scheme involving the energy mismatch $2\Omega_z$ and the interstate coupling $\Omega_x \pm i\Omega_y$.

the geometric vector potential for the optical flux lattices contains gauge-dependent singularities. To avoid these singularities, the previous study³⁹ concentrated on the magnetic flux rather on the vector potential.

The vector potential \mathbf{A} plays an important role in the quantum physics.⁴¹ It is featured in the Pearls substitution^{42,43} widely used in the tight binding models for the particle motion in the magnetic field. Specifically, the tunneling matrix element between the lattice sites \mathbf{r}_A and \mathbf{r}_B acquires the Pearls phase factor proportional to $\int_{\mathbf{r}_A}^{\mathbf{r}_B} \mathbf{A} \cdot d\mathbf{r}$.

Here we explore the optical flux lattices. We analyze not only the magnetic flux³⁹ but also the geometric vector potential generating the flux, as well as the accompanying geometric scalar potential. We show how to deal with the gauge-dependent singularities of the Aharonov-Bohm (AB) type⁴¹ appearing in the vector potentials for the optical flux lattices. We present a way to calculate the continuous magnetic flux through the elementary cell via the singularities of the vector potential inside the cell.

Subsequently we analyze a square optical flux lattice and present a way of creating it using the Raman transitions. A related setup has been proposed recently by Cooper and Dalibard aimed at producing triangular and hexagonal optical flux lattices using three waves propagating at 120 degrees between each other.⁴⁴ To create a square optical flux lattice, we now propose to use a set of properly chosen polarization-dependent standing waves propagating at a right angle and containing a time-phase difference.

2. FORMULATION

2.1 Hamiltonian and its eigenstates

Let us begin with presenting a general formulation of the gauge potentials for the two-level system. Consider the center of mass motion of a two-level atom described by the Hamiltonian¹

$$\hat{H} = \left(\frac{\mathbf{p}^2}{2m} + V \right) \hat{1} + \hat{U}, \quad (1)$$

where $\mathbf{p} = -i\hbar\nabla$ is the atomic momentum, $\hat{1}$ is the identity operator, V is the state-independent external potential, and

$$\hat{U} = -\hbar\boldsymbol{\Omega} \cdot \hat{\boldsymbol{\sigma}} = -\hbar \begin{pmatrix} \Omega_z & \Omega_x - i\Omega_y \\ \Omega_x + i\Omega_y & -\Omega_z \end{pmatrix} \quad (2)$$

is the space-dependent coupling operator determined by the laser fields or other external perturbations. Here the vector $\boldsymbol{\Omega} = (\Omega_x, \Omega_y, \Omega_z)$ defines the coupling between the atomic internal states and $\hat{\boldsymbol{\sigma}} = (\sigma_x, \sigma_y, \sigma_z)$ is the spin 1/2 operator, $\sigma_{x,y,z}$ being the Pauli matrices. As depicted in Fig. 1, the frequency $2\Omega_z$ represents the mismatch between two atomic internal states, whereas $\Omega_x \pm i\Omega_y$ are the transition matrix elements between the two states.

As discussed previously,^{16,39} the two-level atom-light coupling can be engineered using ytterbium atoms containing a metastable excited state. In such a scheme the lasers are used to induce the transitions between the atomic internal states characterized the coupling strengths $\Omega_x + i\Omega_y$, as well as to generate optical potentials. To have potentials with the opposite sign $\pm\Omega_z$ for difference atomic internal states, one should choose an anti-magic

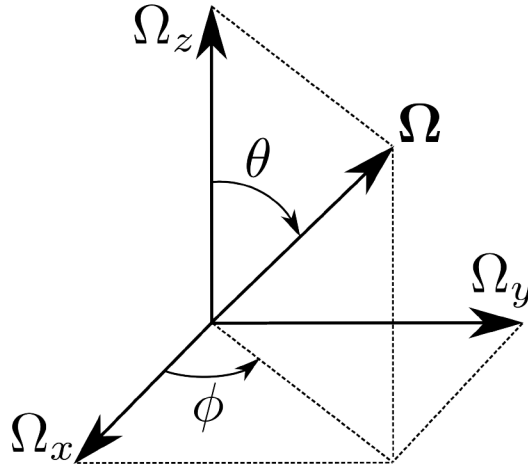


Figure 2. The coupling vector Ω .

wavelength (one which maximizes the differential Stark shift) when optically trapping the atoms. Alternatively, one can use the Raman transition, as will be discussed in more detail below.

It is convenient to parametrize the coupling vector $\mathbf{\Omega} = (\Omega_x, \Omega_y, \Omega_z)$ via the spherical angles θ and ϕ shown in Fig. 2:

$$\tan \phi = \Omega_y / \Omega_x, \quad \cos \theta = \Omega_z / \Omega, \quad \Omega = \sqrt{\Omega_x^2 + \Omega_y^2 + \Omega_z^2}, \quad (3)$$

where $\Omega = |\mathbf{\Omega}|$ is the total coupling strength.

The coupling operator in Eq. (2) has two position-dependent eigenstates $|\pm\rangle \equiv |\pm(\mathbf{r})\rangle$ which can be represented in terms of the angles θ and ϕ

$$|+\rangle = \begin{pmatrix} \cos(\theta/2) \\ e^{i\phi} \sin(\theta/2) \end{pmatrix}, \quad |-\rangle = \begin{pmatrix} -e^{-i\phi} \sin(\theta/2) \\ \cos(\theta/2) \end{pmatrix}, \quad (4)$$

the corresponding energies being

$$E_{\pm} = \pm \hbar \Omega. \quad (5)$$

The eigenstates $|\pm\rangle$ are single-valued everywhere but the south pole of the vector $\mathbf{\Omega}$ where polar angle is $\theta = \pi$, whereas the azimuthal angle ϕ is arbitrary. Alternatively one can choose another set of eigenstates $|\tilde{\pm}\rangle$ which are single-valued everywhere but in the north pole of the vector $\mathbf{\Omega}$ where polar angle is $\theta = 0$ and the azimuthal angle ϕ is arbitrary. The two sets of eigenstates are related via a gauge transformation

$$|\tilde{+}\rangle = |+\rangle e^{-i\phi}, \quad |\tilde{-}\rangle = |-\rangle e^{i\phi}. \quad (6)$$

The different choices of the atomic internal states shown in Eqs. (4) and (6) lead to the geometric vector potentials which are equivalent.

3. GAUGE POTENTIALS

3.1 General

The full state-vector describing both the internal and center of mass motion of an atom is

$$|\Psi(\mathbf{r}, t)\rangle = \sum_{\pm} |\pm\rangle \psi_{\pm}(\mathbf{r}, t)$$

where $\psi_{\pm}(\mathbf{r}, t)$ is the wave-function of the atomic center of mass motion in the atomic internal state $|\pm\rangle \equiv |\pm(\mathbf{r})\rangle$. Suppose that the atom is prepared in the lowest internal state $|\tilde{-}\rangle$. We are interested in a situation where $\Omega \neq 0$

all over the space. Thus the atom-light Hamiltonian [Eq. 2]) has two non-degenerate eigenstates $|\pm\rangle \equiv |\pm(\mathbf{r})\rangle$ at all spatial points. If the characteristic kinetic energy of the atomic center of mass motion is small compared to the energy difference between the two internal states $\Delta E = 2\hbar\Omega$, the internal state of the atom will follow adiabatically atomic lower state and the excited state contribution of $\psi_+(\mathbf{r}, t)$ can be neglected. Projecting the full Schrödinger equation $i\hbar\left|\dot{\Psi}(\mathbf{r}, t)\right\rangle = \hat{H}|\Psi(\mathbf{r}, t)\rangle$ onto the lower energy eigenstate leads to an effective Schrödinger equation for the wave-function for the atomic motion in the lowest internal state:^{1, 19, 22–24}

$$i\hbar\frac{\partial}{\partial t}\psi_-(\mathbf{r}, t) = \left[\frac{(\mathbf{p} - \mathbf{A})^2}{2m} + V - E_- + W \right] \psi_-(\mathbf{r}, t), \quad (7)$$

where the geometric vector and scalar potentials $\mathbf{A} \equiv \mathbf{A}(\mathbf{r})$ and $W \equiv W(\mathbf{r})$ appear due to the position dependence of the atomic internal states:

$$\mathbf{A}(\mathbf{r}) = i\hbar\langle -|\nabla|-\rangle, \quad W(\mathbf{r}) = \frac{\hbar^2}{2m} |\langle +|\nabla|-\rangle|^2. \quad (8)$$

The gauge-independent scalar potential $W(\mathbf{r})$ emerges when eliminating the excited atomic state. It represents the kinetic energy of the oscillatory micromotion due to the tiny transitions to the eliminated state $|+\rangle \equiv |+(\mathbf{r})\rangle$.^{45, 46} On the other hand, the vector potential can be interpreted as a kinetic energy of the atomic center of mass motion associated with the position-dependent internal state $|-\rangle \equiv |-(\mathbf{r})\rangle$. Explicitly the gauge potentials read for the present situation¹

$$\mathbf{A}(\mathbf{r}) = \frac{\hbar}{2}(\cos\theta - 1)\nabla\phi. \quad (9)$$

$$W(\mathbf{r}) = \frac{\hbar^2}{8m} \left[(\nabla\theta)^2 + (\sin\theta\nabla\phi)^2 \right]. \quad (10)$$

It is noteworthy that the vector potential $\mathbf{A}(\mathbf{r})$ contains the Aharonov-Bohm (AB) type fluxes with a single flux quantum at the points where $\cos\theta = 1$, i.e. at the north poles of the coupling vector $\boldsymbol{\Omega}$. On the other hand, the vector potential $\tilde{\mathbf{A}}(\mathbf{r}) = i\hbar\langle \tilde{-}|\nabla|\tilde{-}\rangle$ corresponding to an alternative phase choice of the internal ground state $|\tilde{-}\rangle$, Eq. (6), differs by a gradient of the azimuthal angle $\hbar\nabla\phi$ and contains AB fluxes with a single flux quantum at the south poles of the vector $\boldsymbol{\Omega}$ where $\cos\theta = -1$:

$$\tilde{\mathbf{A}}(\mathbf{r}) = \mathbf{A}(\mathbf{r}) + \hbar\nabla\phi = \frac{\hbar}{2}(\cos\theta + 1)\nabla\phi. \quad (11)$$

and $\tilde{\mathbf{A}}(\mathbf{r})$ are equivalent and produce the same effective magnetic field (the magnetic flux density) $\mathbf{B}(\mathbf{r}) = \nabla \times \mathbf{A}(\mathbf{r}) = \nabla \times \tilde{\mathbf{A}}(\mathbf{r})$

$$\mathbf{B}(\mathbf{r}) = \frac{\hbar}{2}\nabla(\cos\theta) \times \nabla\phi. \quad (12)$$

where the gauge-dependent AB singularities (if any) featured in the vector potentials have been excluded in Eq. (12) for \mathbf{B} . It is convenient to represent the magnetic flux density in terms of the unit vector $\mathbf{N} = \boldsymbol{\Omega}/\Omega$

$$\mathbf{B}(\mathbf{r}) = -\frac{\hbar}{2} \frac{\nabla N_x \times \nabla N_y}{N_z}, \quad (13)$$

Thus if Ω_z alternates the sign at the points where $\Omega_x = 0$ and $\Omega_y = 0$, this might compensate the alternation of the sign of $\nabla N_x \times \nabla N_y$ at these points, giving a non-zero magnetic flux, such as the one given by Eq. (24) below. This shows the necessity to have an oscillating detuning Ω_z in addition to the oscillating coupling $\Omega_x + i\Omega_y$.

Note that the geometric scalar potential can lead to a modification of the overall scalar potential, the most significant modification taking place at the singular points where $\Omega_x + i\Omega_y = 0$ and also at the points of the minimum magnetic flux where $\Omega_z = 0$.

3.2 Periodic atom-light coupling

Suppose now that the coupling vector $\boldsymbol{\Omega} = \boldsymbol{\Omega}(\mathbf{r}) = (\Omega_x, \Omega_y, \Omega_z)$ is a spatially periodic function in the xy plane

$$\boldsymbol{\Omega}(\mathbf{r} + \mathbf{r}_{n,m}) = \boldsymbol{\Omega}(\mathbf{r}), \quad \mathbf{r}_{n,m} = n\mathbf{a}_1 + m\mathbf{a}_2, \quad (14)$$

where \mathbf{a}_1 and \mathbf{a}_2 are the primitive vectors defining a 2D lattice in the xy plane, with n and m being the integers. In that case both the atomic internal dressed states $|\pm\rangle \equiv |\pm(\mathbf{r})\rangle$ and the corresponding geometric potentials $\mathbf{A} \equiv \mathbf{A}(\mathbf{r})$ and $W \equiv W(\mathbf{r})$ are also periodic functions with the same periodicity. Due to the periodicity of the vector potential the total flux over the elementary cell is zero

$$\alpha = \frac{1}{\hbar} \oint_{cell} \mathbf{A} \cdot d\mathbf{r} = \frac{1}{\hbar} \iint_{cell} \mathbf{B}_{tot} \cdot d\mathbf{S} = 0, \quad (15)$$

where

$$\mathbf{B}_{tot} = \mathbf{B}(\mathbf{r}) + \mathbf{B}_{AB}(\mathbf{r})$$

is the total magnetic flux density containing both the continuous (background) magnetic flux density $\mathbf{B}(\mathbf{r})$ and also possibly a set of gauge-dependent singular fluxes of the AB type represented by $\mathbf{B}_{AB}(\mathbf{r})$.

Thus strictly speaking one can not produce a non-zero effective magnetic flux α over the elementary cell using the periodic atom-light coupling. However this does not prevent having a non-staggered continuous magnetic flux density $\mathbf{B}(\mathbf{r})$ over the elementary cell as long as the vector potential contains (gauge-dependent) singularities of the AB type carrying together a non-zero number of the Dirac flux quanta. The AB singularities are associated with the points where the coupling strength $\Omega_x + i\Omega_y$ goes to zero and hence $\cos\theta \rightarrow \pm 1$. Specifically, the vector potential $\mathbf{A}(\mathbf{r})$ can contain the AB singularities in the vicinity of points corresponding to $\cos\theta \rightarrow -1$ for which $\mathbf{A}(\mathbf{r}) \approx -\hbar\nabla\phi$. On the other hand, the transformed vector potential $\tilde{\mathbf{A}}(\mathbf{r})$ becomes singular for $\cos\theta \rightarrow 1$ where $\tilde{\mathbf{A}}(\mathbf{r}) = \hbar\nabla\phi$. Deducing these non-measurable gauge dependent singularities, the resulting flux over the elementary cell is no longer equals to zero

$$\alpha' = \hbar^{-1} \iint_{cell} \mathbf{B} \cdot d\mathbf{S} = -\hbar^{-1} \iint_{cell} \mathbf{B}_{AB}(\mathbf{r}) \cdot d\mathbf{S}. \quad (16)$$

It can be expressed in terms of the vector potential

$$\alpha' = -\hbar^{-1} \sum \oint_{singul} \mathbf{A} \cdot d\mathbf{r} = -\hbar^{-1} \sum \oint_{singul} \tilde{\mathbf{A}} \cdot d\mathbf{r}, \quad (17)$$

where the summation is over the singular points of the vector potential (different for \mathbf{A} and $\tilde{\mathbf{A}}$) around which the contour integration is carried out. Around these singular points the vector potentials reduce to

$$\mathbf{A} \rightarrow -\hbar\nabla\phi, \quad \tilde{\mathbf{A}} \rightarrow \hbar\nabla\phi. \quad (18)$$

Thus each constituent integral provides an integer number of the Dirac flux quanta in Eq. (17). To get non-zero flux α' , the sum of the singular contributions should be non-zero. The flux is maximum if all these singular contributions have the same sign. This is the case for the square flux lattice to be considered next.

To summarize one has the following situation. In the optical flux lattices there is a background non-staggered magnetic field \mathbf{B} plus an array of the gauge-dependent Dirac-string fluxes of the opposite sign. Both fluxes compensate each other so the total magnetic flux over an elementary cell is zero in agreement with the periodicity of the Hamiltonian. However the Dirac-string fluxes are non-measurable and hence are to be excluded. As a result one arrives at a non-staggered magnetic flux over the optical flux lattice.

4. SQUARE OPTICAL FLUX LATTICE

4.1 Adiabatic energies and magnetic flux

Consider the Rabi frequencies of the following form

$$\Omega_x = \Omega_{\perp} \cos(x\pi/a), \quad \Omega_y = \Omega_{\perp} \cos(y\pi/a), \quad \Omega_z = \Omega_{\parallel} \sin(x\pi/a) \sin(y\pi/a). \quad (19)$$

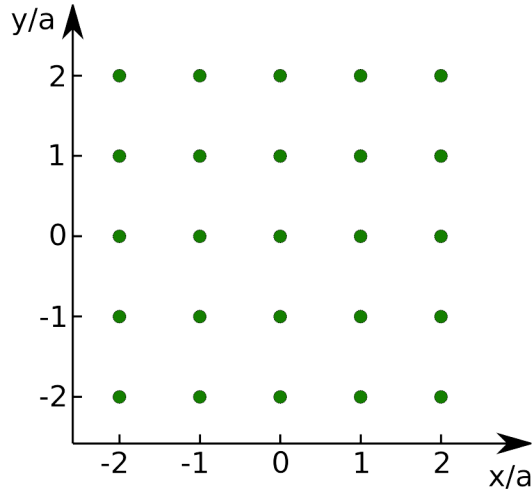


Figure 3. Sites of the square optical flux lattice corresponding to the minima of the adiabatic energy $E_-(x, y)$.

The atom-light coupling has then a periodicity $2a$ in both x and y directions. In the symmetric case, $\Omega_\perp = \Omega_\parallel$, the scheme reduces to the one considered previously in Ref.³⁹ As will be discussed in Sec. 5, the Rabi frequencies given by Eq. (19) can be produced using the the Raman transitions induced by a set of properly chosen polarization-dependent standing waves propagating at a right angle and containing a time-phase difference.

The total Rabi frequency corresponding to Eq. (19) is:

$$\Omega = -\sqrt{\Omega_\parallel^2 + (\Omega_\perp^2 - \Omega_\parallel^2)(f_x^2 + f_y^2) + \Omega_\parallel^2 f_x^2 f_y^2}, \quad f_u = \cos(u\pi/a). \quad (20)$$

so the adiabatic energies $E_\pm = \pm\hbar\Omega$ have a periodicity a which is twice smaller than that of the atom-light coupling.

Assuming that $\Omega_\perp^2 > \Omega_\parallel^2/2$, the minima of the adiabatic energy $E_-(x, y)$ are positioned at $x_n = na$ and $y_m = ma$ (shown by green dots in in Fig. 3) at which $\Omega_z = 0$. On the other hand, the energy maxima are positioned at $x_{n,max} = na + a/2$ and $y_{m,max} = ma + a/2$ where the atom-light coupling vanishes: $\Omega_x + i\Omega_y \rightarrow 0$. Thus one has

$$E_{min} = E_-(na, ma) = -\Omega_\perp\sqrt{2}, \quad E_{max} = E_-(na + a/2, ma + a/2) = -\Omega_\parallel, \quad (21)$$

In the vicinity of the energy maxima we have

$$\Omega_x \approx \Omega_\perp (x - x_{n,max}) (-1)^n, \quad \Omega_y \approx \Omega_\perp (y - y_{m,max}) (-1)^m, \quad \Omega_z \approx \Omega_\parallel (-1)^{n+m}. \quad (22)$$

Thus the angle ϕ does indeed rotate in the same direction around all singularities of the vector potential positioned at $x = x_{n,max}$ and $y = y_{n,max}$ when integrating in Eqs. (16) and (17). This provides a non-zero magnetic flux over an elementary cell to be considered next.

4.2 Vector potential and magnetic flux

Consider the flux over an elementary cell ranging at $0 < x < 2a$ and $0 < y < a$. The vector potential \mathbf{A} has the AB type singularities for $\Omega_z = -1$ corresponding to the odd values of $n + m$ in Eq. (22). Within the elementary cell these are two points positioned at $(n = 0, m = 1)$ and $(n = 1, m = 0)$, each providing a single quantum of the magnetic flux (with a negative sign). Integrating the vector potential around each singular point, Eqs. (17)-(18) yield the background magnetic flux:

$$\alpha' = -\hbar^{-1} \sum \oint_{singul} \mathbf{A} \cdot d\mathbf{r} = -4\pi. \quad (23)$$

In this way a measurable continuous flux over the elementary cell accommodates two Dirac quanta.³⁹ The same magnetic flux α' is obtained using the vector potential \tilde{A} which contains AB singularities at $n = m = 0$ and $n = m = 1$, again each carrying a single Dirac flux quantum with a negative sign.

Using Eq. (13), one arrives at the explicit result for the magnetic flux density

$$\mathbf{B}(\mathbf{r}) = -\frac{\hbar \pi^2}{2 a^2} \frac{1 - \cos^2(x\pi/a) \cos^2(y\pi/a)}{\beta \{1 + \gamma [\cos^2(x\pi/a) + \cos^2(y\pi/a)] + \cos^2(x\pi/a) \cos^2(y\pi/a)\}^{3/2}} \mathbf{e}_z. \quad (24)$$

where $\beta = \Omega_{\parallel}/\Omega_{\perp}$ and $\gamma = (1 - \beta^2)/\beta^2$. Equation (24) demonstrates that the magnetic flux is non-staggered, and its profile can be shaped by changing the ratio of the Rabi frequency amplitudes β . It is evident that the magnetic flux is zero at the potential minima $x_n = na$ and $y_m = ma$ for finite values of β . If $\beta = 1$, Eq. (24) becomes equivalent to the result obtained independently by Jean Dalibard.⁴⁷

4.3 Scalar potential

Assuming $\Omega_{\parallel} = \Omega_{\perp}$, the second term entering the scalar potential [Eq. (10)] is

$$(\sin \theta \nabla \phi)^2 = \left(\frac{\pi}{a}\right)^2 \frac{\cos^2(x\pi/a) \sin^2(y\pi/a) + \cos^2(y\pi/a) \sin^2(x\pi/a)}{[1 + \cos^2(x\pi/a) \cos^2(y\pi/a)] [\cos^2(x\pi/a) + \cos^2(y\pi/a)]} \quad (25)$$

It is evident that $(\sin \theta \nabla \phi)^2$ is zero at the minima of the adiabatic energy $x_n = na$ and $y_m = ma$. On the other hand, it equals to $(\pi/a)^2$ at the maxima of the adiabatic energy $x_{n,max} = na + a/2$ and $y_{m,max} = ma + a/2$. This part of the scalar potential behaves similar to the adiabatic energy $E_-(x, y)$, thus increasing the energy maxima by the amount $(\hbar\pi/a)^2/8m$.

The first terms entering the scalar potential [Eq. (10)] is

$$(\nabla \theta)^2 = \left(\frac{\pi}{a}\right)^2 \frac{g_x^2 + g_y^2}{[1 + \cos^2(x\pi/a) \cos^2(y\pi/a)]^2 [\cos^2(x\pi/a) + \cos^2(y\pi/a)]}. \quad (26)$$

with

$$g_x = \sin(y\pi/a) \cos(x\pi/a) [1 + \cos^2(y\pi/a)] \quad (27)$$

$$g_y = \sin(x\pi/a) \cos(y\pi/a) [1 + \cos^2(x\pi/a)] \quad (28)$$

Thus $(\nabla \theta)^2$ is zero both at the minima and maxima of the adiabatic energy. Yet is equal to $(\pi/a)^2$ if $\cos(x\pi/a) \rightarrow 0$ and $\cos(y\pi/a) \rightarrow 0$, i.e. at the center of the plaquette thus raising the potential there.

In this way the scalar potential is given by Eq. (10) together with Eqs. (25)-(28). It is zero at the corners of a plaquette and reaches its maximum values at the center of the plaquette, thus behaving similar to the magnetic field. In this way the scalar potential pushes the atoms away from the area of the high magnetic field at the center of the plaquette.

5. GENERATION OF THE OPTICAL FLUX LATTICE USING THE RAMAN TRANSITIONS

5.1 Atom-light operator

In a proposal by Cooper and Dalibard⁴⁴ a two-level system is made of two magnetic sublevels coupled by Raman transitions, as shown in Fig. 4. The latter are induced by two laser fields with different frequencies. One of them has all three circular polarizations, the corresponding Rabi frequencies being κ_m with $m = 0, \pm 1$, as shown in the red color in Fig. 4. The second field shown in the green color is in resonance with the Raman transitions between these two levels. It is characterized by the Rabi frequency E and has a circular σ_- polarization. A combined action of the two fields leads to the following effective Hamiltonian for the two-level system composed of the ground states $|g_{\pm}\rangle$:⁴⁴

$$\hat{U} = \frac{\hbar \kappa_{tot}^2}{3\Delta} \hat{I} + \frac{\hbar}{3\Delta} \begin{pmatrix} |\kappa_-|^2 - |\kappa_+|^2 & E\kappa_0 \\ E\kappa_0^* & |\kappa_+|^2 - |\kappa_-|^2 \end{pmatrix} \quad (29)$$

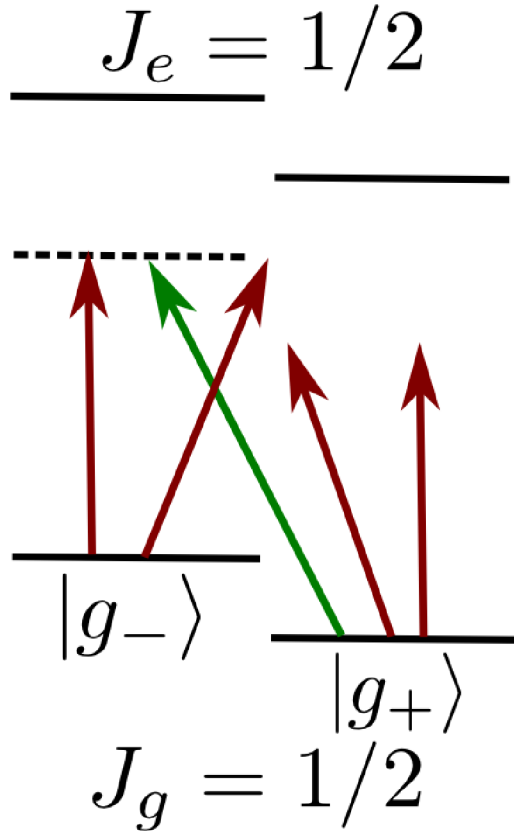


Figure 4. Raman transitions providing the optical flux lattice.

where $\kappa_{tot}^2 = |\kappa_0|^2 + |\kappa_+|^2 + |\kappa_-|^2$ is the modulus square of the total Rabi frequency. Dalibard and Cooper considered a situation where the field κ represents a superposition of three linearly polarized plane waves.⁴⁴ In that case one can produce a triangular or hexagonal lattices.

5.2 Standing-wave setup produced by four running waves

The square optical flux lattice can be formed if the field κ is given by

$$\kappa = 2K [\cos(kx) + i \cos(ky)] \mathbf{e}_z \cos \theta + 2K [\sin(ky) \mathbf{e}_x - i \sin(kx) \mathbf{e}_y] \sin \theta. \quad (30)$$

Equation (30) represents a sum of polarization-dependent standing waves with a $\pi/2$ time-phase difference (represented by the imaginary unit) between the waves propagating in the x and y directions. Note that the standing waves with time-phase difference were studied previously in the context of the light forces.^{48,49} The quantities entering the atom-light coupling operator [Eq. (29)] are now

$$E\kappa_0 = 2KE [\cos(kx) + i \cos(ky)] \cos \theta, \quad (31)$$

$$|\kappa_-|^2 - |\kappa_+|^2 = -4K^2 \sin(ky) \sin(kx) \sin^2 \theta \quad (32)$$

and

$$\kappa_{tot}^2 = 4K^2 \{ [\cos^2(kx) + \cos^2(ky)] (1 - 2 \sin^2 \theta) + \sin^2 \theta \}. \quad (33)$$

The atom-light Hamiltonian [Eq. (29)] can be rewritten as

$$\hat{U} = \hbar\Omega_I \hat{I} - \hbar\mathbf{\Omega} \cdot \hat{\sigma}. \quad (34)$$

where

$$\Omega_x = b\Omega_{\parallel} \cos(x\pi/a), \quad \Omega_y = b\Omega_{\parallel} \cos(y\pi/a), \quad \Omega_z = \Omega_{\parallel} \sin(x\pi/a) \sin(y\pi/a) \quad (35)$$

and

$$\Omega_I = c\Omega_{\parallel} [\cos^2(kx) + \cos^2(ky)] + const,$$

with

$$\Omega_{\parallel} = \frac{4\hbar K^2}{3\Delta}, \quad b = -\frac{E \cos \theta}{2K}, \quad c = 1 - 2 \sin^2 \theta.$$

If $\theta = \pm\pi/4$, the state-independent potential is constant ($c = 0$, so $\Omega_I = const$), and the situation reduces to the one analyzed in the previous Section. If additionally $b = 1$, one arrives at a atom-light coupling considered by Cooper.³⁹ On the other hand, if $\theta \neq \pm\pi/4$, the state-independent potential is no longer constant. Furthermore the sign of the position-dependent part of the potential Ω_I can be controlled. If $|\theta| > \pi/4$, the parameter $c > 0$, whereas for $|\theta| < \pi/4$, one has $c < 0$. The change in the sign of the parameter c can lead to a significant reshaping of the optical potential minima of the optical flux lattices.

6. CONCLUDING REMARKS

We have explored the optical flux lattices produced for ultra-cold atoms in the radiation field when both the atom-light coupling and the detuning exhibit an oscillatory behavior. We have analyzed not only the magnetic flux but also the geometric vector potential generating the flux, as well as the accompanying geometric scalar potential. We have show how to deal with the gauge-dependent singularities of the Aharonov-Bohm (AB) type appearing in the vector potentials for the optical flux lattices. We have present a way to calculate the continuous magnetic flux through the elementary cell via the singularities of the vector potential inside the cell. The analysis is illustrated with a square optical flux lattice. We have presented a way of creating such a lattice using the Raman transitions induced by a set of properly chosen polarization-dependent standing waves propagating at a right angle and containing a time-phase difference.

ACKNOWLEDGMENTS

The author acknowledge helpful discussions with Jean Dalibard, Nigel Cooper, Tilman Esslinger, and Janne Ruostekoski. G.J. acknowledges the financial support of the EU FP7 project NAMEQUAM. I.B.S. acknowledge the financial support of the NSF through the PFC at JQI, and the ARO with funds from both the Atomtronics MURI and the DARPA OLE program.

REFERENCES

- [1] Dalibard, J., Gerbier, F., G.Juzeliūnas, and P.Öhberg, “Artificial gauge potentials for neutral atoms,” *Rev. Mod. Phys.* **83**, 1523 (2011).
- [2] Lewenstein, M., Sanpera, A., Ahufinger, V., Damski, B., De, A. S., and Sen, U., “Ultracold atomic gases in optical lattices: mimicking condensed matter physics and beyond,” *Adv. Phys.* **56**(2), 243–379 (2007).
- [3] Ketterle, W. and Zwerlein, M., [*in Ultra Cold Fermi Gases*], vol. CLXIV of *Proceedings of the International School of Physics “Enrico Fermi”*, Edts M. Inguscio, W. Ketterle and C. Salomon, IOS Press (2007).
- [4] Bloch, I., Dalibard, J., and Zwerger, W., “Many-body physics with ultracold gases,” *Rev. Mod. Phys.* **80**(3), 885 (2008).
- [5] Giorgini, S., Pitaevskii, L. P., and Stringari, S., “Theory of ultracold atomic fermi gases,” *Rev. Mod. Phys.* **80**(4), 1215 (2008).
- [6] Greiner, M., Mandel, M. O., Esslinger, T., Hänsch, T., and Bloch, I., “Quantum phase transition from a superfluid to a mott insulator in a gas of ultracold atoms,” *Nature* **415**, 39 (2002).
- [7] Hadzibabic, Z., Krüger, P., Cheneau, M., Battelier, B., and Dalibard, J., “Berezinskii-Kosterlitz-Thouless crossover in a trapped atomic gas,” *Nature* **441**, 1118–1121 (2006).
- [8] von Klitzing, K., “The quantized hall effect,” *Rev. Mod. Phys.* **519**, 1986 (1986).
- [9] Cooper, N. R., “Rapidly rotating atomic gases,” *Advances in Physics* **57**(6), 539–616 (2008).
- [10] Fetter, A. L., “Rotating trapped bose-einstein condensates,” *Rev. Mod. Phys.* **81**, 647–691 (May 2009).

- [11] Jaksch, D. and Zoller, P., “Creation of effective magnetic fields in optical lattices: the Hofstadter butterfly for cold neutral atoms,” *New Journal of Physics* **5**, 56.1 (2003).
- [12] Mueller, E. J., “Artificial electromagnetism for neutral atoms: Escher staircase and Laughlin liquids,” *Phys. Rev. A* **70**, 041603 (Oct 2004).
- [13] Sørensen, A. S., Demler, E., and Lukin, M. D., “Fractional quantum hall states of atoms in optical lattices,” *Phys. Rev. Lett.* **94**, 086803 (Mar 2005).
- [14] Osterloh, K., Baig, M., Santos, L., Zoller, P., and Lewenstein, M., “Cold atoms in non-abelian gauge potentials: From the Hofstadter moth to lattice gauge theory,” *Phys. Rev. Lett.* **95**, 010403 (Jun 2005).
- [15] Lim, L.-K., Smith, C. M., and Hemmerich, A., “Staggered-vortex superfluid of ultracold bosons in an optical lattice,” *Phys. Rev. Lett.* **100**(13), 130402 (2008).
- [16] Gerbier, F. and Dalibard, J., “Gauge fields for ultracold atoms in optical superlattices,” *New Journal of Physics* **12**(3), 033007 (2010).
- [17] Kolovsky, A. R., “Creating artificial magnetic fields for cold atoms by photon-assisted tunneling,” *Europhys. Lett.* **93**, 20003 (2011).
- [18] Berry, M. V., “Quantal phase factors accompanying adiabatic changes,” *Proc. Roy. Soc. London A* **392**, 45–57 (1984).
- [19] Jackiw, R. *Comments At. Mol. Phys.* **21**, 71 (1988).
- [20] Moody, J., Shapere, A., and Wilczek, F., “Realizations of magnetic-monopole gauge fields: Diatoms and spin precession,” *Phys. Rev. Lett.* **56**(9), 893 (1986).
- [21] Zee, A., “Non-abelian gauge structure in nuclear quadrupole resonance,” *Phys. Rev. A* **38**(1), 1 (1988).
- [22] Shapere, A. and Wilczek, F., eds., [*Geometric Phases in Physics*], World Scientific, Singapore (1989).
- [23] Mead, C. A., “The geometric phase in molecular physics,” *Rev. Mod. Phys.* **84**, 51 (1992).
- [24] Bohm, A., Mostafazadeh, A., Koizumi, H., Niu, Q., and Zwanziger, J., [*Geometric Phases in Quantum Systems*], Springer, Berlin, Heidelberg, New York (2003).
- [25] Xiao, D., Chang, M.-C., and Q. Niu, “Berry phase effects on electronic properties,” *Rev. Mod. Phys.* **82**, 1959 (2010).
- [26] Dum, R. and Olshanii, M., “Gauge structures in atom-laser interaction: Bloch oscillations in a dark lattice,” *Phys. Rev. Lett.* **76**, 1788–1791 (Mar 1996).
- [27] Visser, P. M. and Nienhuis, G., “Geometric potentials for subrecoil dynamics,” *Phys. Rev. A* **57**, 4581–4591 (Jun 1998).
- [28] Dutta, S. K., Teo, B. K., and Raithel, G., “Tunneling dynamics and gauge potentials in optical lattices,” *Phys. Rev. Lett.* **83**, 1934–1937 (Sep 1999).
- [29] Juzeliūnas, G., Öhberg, P., Ruseckas, J., and Klein, A., “Effective magnetic fields in degenerate atomic gases induced by light beams with orbital angular momenta,” *Phys. Rev. A* **71**, 053614 (May 2005).
- [30] Ruseckas, J., Juzeliūnas, G., Öhberg, P., and Fleischhauer, M., “Non-abelian gauge potentials for ultracold atoms with degenerate dark states,” *Phys. Rev. Lett.* **95**, 010404 (Jun 2005).
- [31] Juzeliūnas, G., Ruseckas, J., Öhberg, P., and Fleischhauer, M., “Light-induced effective magnetic fields for ultracold atoms in planar geometries,” *Phys. Rev. A* **73**, 025602 (Feb 2006).
- [32] Zhu, S.-L., Fu, H., Wu, C.-J., Zhang, S.-C., and Duan, L.-M., “Spin hall effects for cold atoms in a light-induced gauge potential,” *Phys. Rev. Lett.* **97**, 240401 (2006).
- [33] Günter, K. J., Cheneau, M., Yefsah, T., Rath, S. P., and Dalibard, J., “Practical scheme for a light-induced gauge field in an atomic Bose gas,” *Phys. Rev. A* **79**, 011604 (2009).
- [34] Cooper, N. R. and Hadzibabic, Z., “Measuring the superfluid fraction of an ultracold atomic gas,” *Phys. Rev. Lett.* **104**(3), 030401 (2010).
- [35] Spielman, I. B., “Raman processes and effective gauge potentials,” *Phys. Rev. A* **79**, 063613 (Jun 2009).
- [36] Lin, Y.-J., Compton, R. L., Jiménez-García, K., Porto, J. V., and Spielman, I. B., “Synthetic magnetic fields for ultracold neutral atoms,” *Nature* **462**, 628–632 (2009).
- [37] Lin, Y. J., Compton, R. L., Perry, A. R., Phillips, W. D., Porto, J. V., and Spielman, I. B., “Bose-einstein condensate in a uniform light-induced vector potential,” *Phys. Rev. Lett.* **102**, 130401 (2009).
- [38] Laughlin, R. B., “Nobel lecture : fractional quantization,” *Rev. Mod. Phys.* **71**, 863 (1999).

- [39] Cooper, N., "Optical flux lattices for ultracold atomic gases," *Phys. Phys. Lett.* **106**, 175301 (2011).
- [40] Spielman, I., "An optical lattice of flux," *Physics* **4**, 35 (2011).
- [41] Aharonov, Y. and Bohm, D., "Significance of electromagnetic potentials in quantum theory," *Phys. Rev.* **115**, 485 (1959).
- [42] Peierls, R. *Z. Phys.* **80**, 763 (1933).
- [43] Luttinger, J. M., "The effect of a magnetic field on electrons in a periodic potential," *Phys. Rev.* **84**, 814–817 (Nov 1951).
- [44] Cooper, N. R. and Dalibard, J., "Optical flux lattices for two-photon dressed states," *arXiv:1106.0820*.
- [45] Aharonov, Y. and Stern, A., "Origin of the geometric forces accompanying berry's geometric potentials," *Phys. Rev. Lett.* **69**(25), 3593–3597 (1992).
- [46] Cheneau, M., Rath, S. P., Yefsah, T., Günter, K. J., Juzeliūnas, G., and Dalibard, J., "Geometric potentials in quantum optics: A semi-classical interpretation," *Europhys. Lett.* **83**(6), 60001 (2008).
- [47] Dalibard, J. unpublished (2011).
- [48] Hemmerich, A., Donald Schropp, J., and Hänsch, T. W., "Light forces in two crossed standing waves with controlled time-phase difference," *Phys. Rev. A* **44**, 1910 (1991).
- [49] Hemmerich, A., Schropp, D., Esslinger, T., and Hansch, T. W., "Elastic scattering of rubidium atoms by two crossed standing waves," *Europhys. Lett.* **18**, 391 (1992).